Surface Rashba-Edelstein Spin-Orbit Torque Revealed by Molecular Self-Assembly

Satoshi Haku,[1,*] Atsushi Ishikawa,[2] Akira Musha,[1] Hiroyasu Nakayama,[3] Takashi Yamamoto,[4] and Kazuya Ando[1,5,6,†]

[1] *Department of Applied Physics and Physico-Informatics, Keio University, Yokohama 223-8522, Japan*
[2] *Center for Green Research on Energy and Environmental Materials, National Institute for Materials Science, Tsukuba 305-0044, Japan*
[3] *International Center for Young Scientists, National Institute for Materials Science, Tsukuba 305-0047, Japan*
[4] *Department of Chemistry, Keio University, Yokohama 223-8522, Japan*
[5] *Keio Institute of Pure and Applied Science (KiPAS), Keio University, Yokohama 223-8522, Japan*
[6] *Center for Spintronics Research Network (CSRN), Keio University, Yokohama 223-8522, Japan*

(Received 10 April 2019; revised manuscript received 6 April 2020; accepted 13 April 2020; published 27 April 2020)

We report the observation of a spin-orbit torque (SOT) originating from the surface Rashba-Edelstein effect. We find that the SOT in a prototypical spin-orbitronic system, a Pt/Co bilayer, can be manipulated by molecular self-assembly on the Pt surface. This provides evidence that the Rashba spin-orbit coupling at the Pt surface generates a sizable SOT, which is hidden by the strong bulk and interface spin-orbit coupling. We show that the molecular tuning of the surface Rashba-Edelstein SOT is consistent with density-functional-theory calculations. These results illustrate the crucial role of the surface spin-orbit coupling in the SOT generation, which alters the landscape of metallic spin-orbitronic devices.

DOI: 10.1103/PhysRevApplied.13.044069

I. INTRODUCTION

Spin-orbit coupling is central to magnetism and spintronics [1–6]. It describes the relativistic interaction between the electrons' spin and momentum degrees of freedom, which has a dramatic impact on both the equilibrium and nonequilibrium properties of condensed matter. Of particular recent interest is the interplay between spin-orbit coupling and space-inversion symmetry, which triggers a variety of phenomena, such as chiral spin textures and spin-momentum locking [7,8]. In systems with broken-inversion symmetry, the spin-orbit coupling lifts the electron-spin degeneracy [9]. This phenomenon, termed the Rashba effect, has been observed across various surfaces and interfaces [10–13].

The Rashba effect couples the spin and charge transport through spin-momentum locking; an in-plane charge current induces a transverse spin accumulation [14,15]. This phenomenon, the Rashba-Edelstein effect or the inverse-spin galvanic effect, can generate spin-orbit torques (SOTs), which allow electric manipulation of the magnetization in metallic heterostructures [16–20]. A prototypical spin-orbitronic system is a Pt/Co bilayer, where the strong spin-orbit coupling of the most fundamental charge-spin converter, Pt, plays a key role in the generation of the SOT. The SOT in such spin-orbitronic devices is expected to be generated by the surface, bulk, and interface spin-orbit coupling. However, the SOT has been generally attributed to two mechanisms: the interface Rashba-Edelstein effect and bulk spin Hall effect [5,21,22]. Despite the extensive studies on the SOT over the past decade, the SOT originating from the surface Rashba-Edelstein effect has been neglected.

In this paper, we report the observation of the SOT arising from the surface Rashba-Edelstein effect: the surface Rashba-Edelstein SOT. The crucial evidence is obtained by using the molecular tuning of the Rashba-Edelstein effect [23]. Using the molecular tuning as a tool to study the SOT, we find that the dampinglike (DL) SOT in a Pt/Co bilayer is manipulated by decorating the Pt surface with self-assembled organic monolayers, while the fieldlike (FL) SOT is unaffected by the molecular self-assembly. This result is consistent with the prediction of the SOT arising from the surface Rashba-Edelstein effect and the spin-transfer mechanism, illustrating the crucial role of surface spin-orbit coupling in spin-orbitronic devices.

II. EXPERIMENTAL METHODS

The molecular tuning of the surface Rashba-Edelstein effect is demonstrated by measuring the SOTs in Pt/Co

*56white43@keio.jp
†ando@appi.keio.ac.jp

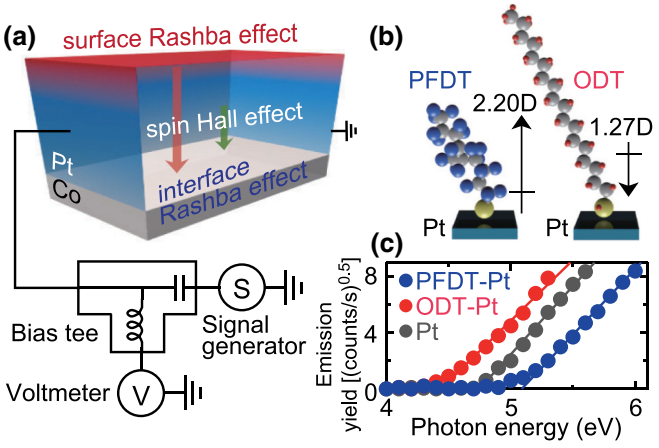

FIG. 1. (a) A schematic illustration of the Pt/Co bilayer and the experimental setup. (b) A schematic illustration of 1-octadecanethiol (ODT) and 1*H*,1*H*,2*H*,2*H*-perfluorodecanethiol (PFDT) molecules on the Pt surface. The arrows represent the dipole moment of the self-assembled-monolayer-(SAM) forming molecules [23]. (c) The square root of the photoelectron emission yield as a function of the scan energy, measured with an atmospheric photoelectron spectrometer for pristine Pt/Co (black), ODT-Pt/Co (red), and PFDT-Pt/Co (blue). The solid lines are linear fits, from which the baseline intercept gives the work function.

bilayers using spin-torque ferromagnetic resonance (ST-FMR). Figure 1(a) shows a schematic illustration of the device structure. The bilayers are fabricated by radio-frequency (rf) magnetron sputtering. First, a Co layer with thickness of t_{Co} is grown on a thermally oxidized Si substrate. Then, on the top of the Co layer, a 1-nm-thick Pt layer is sputtered without breaking the vacuum. To study the effect of the decoration of organic monolayers on the surface of the Pt layer, we use 2 mM solutions of 1-octadecanethiol (ODT) and 1*H*,1*H*,2*H*,2*H*-perfluorodecanethiol (PFDT) in ethanol. The Pt/Co films are immersed in the solution for 20 h at room temperature, which results in the formation of self-assembled monolayers (SAMs) on the surface of the ultrathin-Pt layer [see Fig. 1(b)] [25–30]. The SAM formation is confirmed by the change of the work function Φ. Figure 1(c) shows that the ODT formation decreases Φ, whereas the PFDT formation increases Φ. This result is consistent with the opposite dipoles of ODT and PFDT molecules, since the change in the metal work function is associated with the dipole moment of the SAM-forming molecule perpendicular to the surface [26]. The SAM formation is also confirmed by x-ray photoelectron spectroscopy (see the Supplemental Material [31]).

For the ST-FMR measurement, the Pt/Co films are patterned into rectangular strips with widths of 10 μm and lengths of 100 μm by photolithography and Ar ion etching. Along the longitudinal direction of the Pt/Co device, an rf current with a frequency of f is applied and an in-plane external field H is applied at an angle of 45° with respect to the longitudinal direction of the device. In the Pt/Co bilayer, the rf current flowing in the Pt layer generates DL- and FL-SOTs, as well as an Oersted field, which excite magnetization precession in the Co layer under the FMR condition: $(2\pi f/\gamma) = \sqrt{\mu_0 H_{\mathrm{FMR}}(\mu_0 H_{\mathrm{FMR}} + \mu_0 M_{\mathrm{eff}})}$, where γ is the gyromagnetic ratio, H_{FMR} is the FMR field, and M_{eff} is the effective demagnetization field [32]. The magnetization precession generates a direct-current (dc) voltage V_{mix} through the mixing of the rf charge current and the oscillating resistance due to the anisotropic magnetoresistance (AMR) in the Co layer [33,34]:

$$V_{\mathrm{mix}} = V_{\mathrm{sym}}\frac{W^2}{(\mu_0 H - \mu_0 H_{\mathrm{FMR}})^2 + W^2} + V_{\mathrm{anti}}\frac{W(\mu_0 H - \mu_0 H_{\mathrm{FMR}})}{(\mu_0 H - \mu_0 H_{\mathrm{FMR}})^2 + W^2}, \quad (1)$$

where W is the spectral width. In the ST-FMR signal, the magnitude of the symmetric component V_{sym} is proportional to the DL spin-orbit effective field H_{DL} [35],

$$V_{\mathrm{sym}} = I_{\mathrm{rf}}\Delta R \mu_0 H_{\mathrm{DL}}\zeta\sqrt{\frac{\mu_0 H_{\mathrm{FMR}}}{\mu_0 H_{\mathrm{FMR}} + \mu_0 M_{\mathrm{eff}}}}, \quad (2)$$

where $\zeta = (\mu_0 H_{\mathrm{FMR}} + \mu_0 M_{\mathrm{eff}})/[2\sqrt{2}W(2\mu_0 H_{\mathrm{FMR}} + \mu_0 M_{\mathrm{eff}})]$. I_{rf} and ΔR are the rf current and the resistance change due to the AMR in the bilayer, respectively. The magnitude of the antisymmetric component V_{anti} is proportional to the sum of the FL spin-orbit effective field H_{FL} and the Oersted field $H_{\mathrm{Oe}} = j_c^{\mathrm{Pt}} t_{\mathrm{Pt}}/2$, where t_{Pt} is the thickness of the Pt layer and j_c^{Pt} is the charge current density in the Pt layer [35]:

$$V_{\mathrm{anti}} = I_{\mathrm{rf}}\Delta R(\mu_0 H_{\mathrm{FL}} + \mu_0 H_{\mathrm{Oe}})\zeta. \quad (3)$$

In a system in which H_{FL} is negligible compared to H_{Oe}, the DL-SOT efficiency corresponds to the FMR spin-torque generation efficiency, defined as [33]

$$\xi_{\mathrm{FMR}} = \frac{V_{\mathrm{sym}}}{V_{\mathrm{anti}}}\frac{e\mu_0 M_s t_{\mathrm{Co}} t_{\mathrm{Pt}}}{\hbar}\sqrt{1 + \frac{\mu_0 M_{\mathrm{eff}}}{\mu_0 H_{\mathrm{FMR}}}}, \quad (4)$$

where t_{Pt} is the thickness of the Pt layer and M_s is the saturation magnetization of the Co layer. However, previous studies have shown that a sizable FL-SOT is generated by the Rashba-Edelstein effect at the Co/Pt interface [32,36]. In the presence of a non-negligible FL-SOT, the

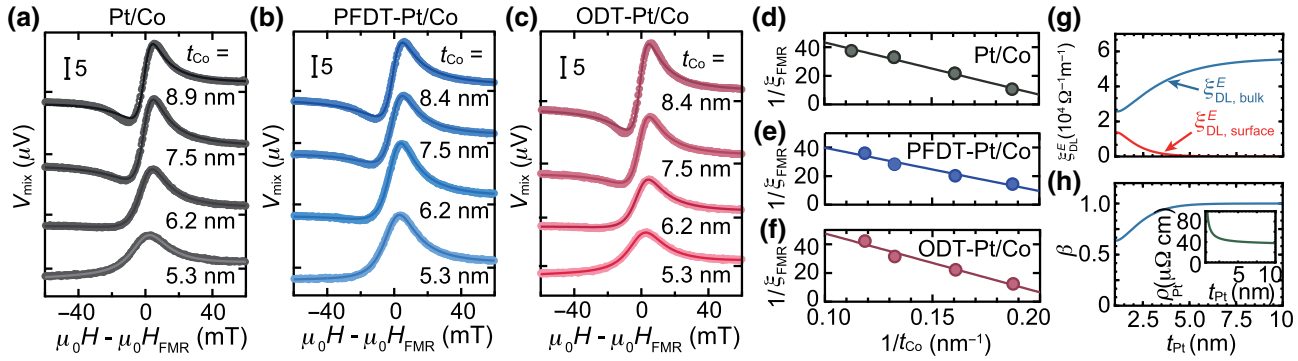

FIG. 2. The spin-torque ferromagnetic resonance (ST-FMR) spectra for the (a) Pt/Co, (b) PFDT-Pt/Co, and (c) ODT-Pt/Co films at $f = 10.3$ GHz, where t_{Co} is the thickness of the Co layer. The open circles are the experimental data and the solid curves are the fitting results using the sum of the symmetric and antisymmetric functions. The $1/t_{Co}$ dependence of $1/\xi_{FMR}$ for the (d) Pt/Co, (e) PFDT-Pt/Co, and (f) ODT-Pt/Co films. The solid circles are the experimental data. The solid lines are the linear fitting results using Eq. (6). (g) The Pt-layer thickness t_{Pt} dependence of $\xi^E_{DL,surface}$ and $\xi^E_{DL,bulk}$, calculated using Eqs. (7) and (8), respectively, for Pt/Co films. (h) The t_{Pt} dependence of $\beta = \xi^E_{DL,bulk}/(\xi^E_{DL,bulk} + \xi^E_{DL,surface})$. The inset shows the t_{Pt} dependence of the Pt-layer resistivity ρ_{Pt}, calculated using a model that takes into account the carrier scatterings at film surfaces and grain boundaries with the parameters $p = 0.97$, $\rho_\infty = 31$ $\mu\Omega$ cm, $\lambda = 10$ nm, and $\zeta = 0.25$ (for details, see Ref. [24]).

determination of the DL- and FL-SOT efficiencies,

$$\xi^E_{DL(FL)} = \left(\frac{2e}{\hbar}\right)\mu_0 M_s t_{Co}\frac{H_{DL(FL)}}{E}, \tag{5}$$

requires disentanglement of H_{FL} and H_{Oe} in the ST-FMR signal, where E is the applied electric field. This is possible by measuring the ST-FMR with various values of t_{Co} because of the different t_{Co} dependence of H_{Oe} and H_{FL}; H_{Oe} is independent of t_{Co}, while H_{FL} decreases with t_{Co}. Under the assumption that $\xi^E_{DL(FL)}$ does not have a strong dependence on t_{Co} in the range examined, $\xi^E_{DL(FL)}$ can be determined from the t_{Co} dependence of ξ_{FMR}, using [32]

$$\frac{1}{\xi_{FMR}} = \frac{1}{\xi^E_{DL}}\left(\frac{1}{\rho_{Pt}} + \frac{\hbar}{e}\frac{\xi^E_{FL}}{4\pi M_s t_{Co} t_{Pt}}\right), \tag{6}$$

where ρ_{Pt} is the resistivity of the Pt layer.

III. MOLECULAR TUNING OF SURFACE RASHBA-EDELSTEIN SPIN-ORBIT TORQUE

In Figs. 2(a)–2(c), we show the V_{mix} signals for various values of t_{Co}, measured using a bias tee at room temperature. We also show $1/\xi_{FMR}$ as a function of $1/t_{Co}$ for the Pt/Co bilayers in Figs. 2(d)–2(f). Using this result with Eq. (6), we determine ξ^E_{DL} and ξ^E_{FL} for the Pt/Co, ODT-decorated Pt/Co (ODT-Pt/Co), and PFDT-decorated Pt/Co (PFDT-Pt/Co) films.

Our finding is that only the DL-SOT is modulated by the molecular self-assembly. From the $1/t_{Co}$ dependence of $1/\xi_{FMR}$, we obtain the DL- and FL-SOT efficiencies, ξ^E_{DL} and ξ^E_{FL}, for the Pt/Co bilayers, as shown in Table I. The obtained values for the pristine Pt/Co bilayer are consistent with the literature values [36]. Here, we note that ξ^E_{FL} is almost unchanged by the SAM formation, as shown in Table I. The change of ξ^E_{FL} due to molecular self-assembly is less than 3%, which is within the experimental error. In contrast, ξ^E_{DL} is manipulated by the molecular decoration; the PFDT formation enhances ξ^E_{DL} by 14%, while the ODT formation suppresses ξ^E_{DL} by 10%.

In the Pt/Co bilayer, the SOTs can be generated by (i) the spin Hall effect in the Pt layer, (ii) the Rashba-Edelstein effect at the Pt/Co interface, and (iii) the Rashba-Edelstein effect at the Pt surface. The spin Hall effect and the surface Rashba-Edelstein effect generate SOTs through the spin-transfer mechanism. In this picture, the ratio of the DL and FL components roughly matches the ratio between the real and imaginary parts of the spin-mixing conductance and thus the dominant component of the SOT in metallic bilayers is the DL-SOT [37]. In contrast, the interface Rashba-Edelstein effect primary exerts a torque on the magnetization at the interface through the exchange coupling. In this scenario, the FL-SOT is much greater than

TABLE I. The summarized parameters for the pristine and SAM-decorated Pt/Co films: the DL-SOT efficiency ξ^E_{DL}, the FL-SOT efficiency ξ^E_{FL}, the resistivity ρ_{Pt} of the Pt layer, and the work function Φ. The Pt resistivity ρ_{Pt} is determined from the measured resistance of the pristine and SAM-decorated Pt/Co films based on a parallel-circuit model with the measured resistivity of the Co layer, $\rho_{Co} = 42.1$ $\mu\Omega$cm.

	Pt/Co	PFDT-Pt/Co	ODT-Pt/Co
ξ^E_{DL} (10^4 Ω^{-1}m^{-1})	3.79 ± 0.17	4.33 ± 0.14	3.42 ± 0.19
ξ^E_{FL} (10^4 Ω^{-1}m^{-1})	2.50 ± 0.17	2.58 ± 0.15	2.55 ± 0.17
ρ_{Pt} ($\mu\Omega$ cm)	84.7 ± 4.0	84.9 ± 2.3	85.3 ± 4.1
Φ (eV)	4.7 ± 0.2	5.0 ± 0.2	4.4 ± 0.4

the DL-SOT, especially in the thin-heavy-metal-layer limit [37]. Thus, in the ultrathin-Pt/Co bilayer, the DL-SOT can be attributed to the bulk spin Hall effect and the surface Rashba-Edelstein effect, while the FL-SOT is dominated by the interface Rashba-Edelstein effect. The interface-dominated FL-SOT is consistent with the fact that $\xi^E_{\rm FL}$ is unchanged by the molecular self-assembly; because the charge screening length in Pt is less than 0.5 Å, the Pt/Co interface, as well as the Co layer, cannot be affected by the ODT and PFDT formation on the Pt surface. Here, in the Pt/Co bilayer, there is a possibility that part of the Co layer is exposed to the surface due to a possible discontinuity of the thin Pt layer. The Rashba-Edelstein effect at the Co surface can also generate the FL-SOT [38]. The negligible change of $\xi^E_{\rm FL}$ indicates that the effect of the SAM formation on the bare Co surface is also negligible in the observed molecular tuning of the SOT.

The observed change of the DL-SOT induced by molecular self-assembly originates from the molecular tuning of the surface Rashba-Edelstein effect in the Pt/Co bilayer. We note that the electron transport in the bulk of the Pt layer is also unaffected by the SAM formation, which is evidenced by the negligible change of the resistivity $\rho_{\rm Pt}$ or the carrier density of the Pt layer after the formation of the ODT and PFDT, as shown in Table I. The change of $\rho_{\rm Pt}$ due to the SAM formation is less than 1%. This indicates that the observed change of $\xi^E_{\rm DL}$ cannot be attributed to the change of the bulk spin Hall effect, since the spin Hall effect can be changed through the change of the carrier density, or $\rho_{\rm Pt}$ [39]. Since the spin Hall effect, as well as the interface Rashba-Edelstein effect, is unaffected by the SAM formation, the change of $\xi^E_{\rm DL}$ can only be attributed to the change of the DL-SOT arising from the Rashba-Edelstein effect at the Pt surface, tuned by the molecular self-assembly.

The observed modulation of the SOT induced by the molecular self-assembly indicates that the surface Rashba-Edelstein effect generates a sizable SOT in the ultrathin-Pt/Co bilayers. Under the assumption that the DL-SOT is generated by the spin-transfer mechanism, the measured $\xi^E_{\rm DL}$ can be decomposed into two terms: $\xi^E_{\rm DL} = \xi^E_{\rm DL,bulk} + \xi^E_{\rm DL,surface}$, where $\xi^E_{\rm DL,bulk}$ and $\xi^E_{\rm DL,surface}$ are the DL-SOT efficiencies due to the bulk spin Hall effect and the surface Rashba-Edelstein effect, respectively. The DL-SOT efficiency due to the spin Hall effect is expressed as [36]

$$\xi^E_{\rm DL,bulk} = \frac{2e}{\hbar}\sigma_{\rm SH}\left[1 - {\rm sech}\left(\frac{t_{\rm Pt}}{\lambda_{\rm Pt}}\right)\right] \times \left[1 + \frac{\sigma_{\rm Pt}\tanh\left(t_{\rm Pt}/\lambda_{\rm Pt}\right)}{2\lambda_{\rm Pt}G_r}\right]^{-1}, \quad (7)$$

where $\sigma_{\rm SH}$, $\sigma_{\rm Pt}$, and $\lambda_{\rm Pt}$ are the spin Hall conductivity, the conductivity, and the spin-diffusion length of the Pt layer, respectively. $G_{\rm r}$ is the real part of the spin-mixing conductance. Using Eq. (7) with $G_{\rm r} = 0.59 \times 10^{15}\ \Omega^{-1}{\rm m}^{-1}$, $\sigma_{\rm SH} = 1.8 \times 10^5\ \Omega^{-1}{\rm m}^{-1}$ and $\lambda_{\rm Pt}/\sigma_{\rm Pt} = 0.77 \times 10^{-15}\ \Omega{\rm m}^2$ [36,40], we obtain $\xi^E_{\rm DL,bulk} = 2.42 \times 10^4\ \Omega^{-1}{\rm m}^{-1}$. For the ultrathin-Pt/Co bilayer, from the measured $\xi^E_{\rm DL}$ we obtain the DL-SOT efficiency due to the surface Rashba-Edelstein effect in the Pt/Co bilayer as $\xi^E_{\rm DL,surface} = \xi^E_{\rm DL} - \xi^E_{\rm DL,bulk} = 1.37 \times 10^4\ \Omega^{-1}{\rm m}^{-1}$. Here, $\xi^E_{\rm DL,surface}$ is proportional to the conversion efficiency from the applied two-dimensional (2D) charge current $j_{\rm c}^{\rm 2D}$ into the three-dimensional (3D) spin current $j_{\rm s}^{\rm 3D}$, $q_{\rm REE} = j_{\rm s}^{\rm 3D}/j_{\rm c}^{\rm 2D}$, due to the Rashba-Edelstein effect (REE) at the Pt surface as [41]

$$\xi^E_{\rm DL,surface} = \frac{(2\lambda_{\rm Pt}/\sigma_{\rm Pt})G_{\rm r}{\rm sech}\left(t_{\rm Pt}/\lambda_{\rm Pt}\right)}{1 + (2\lambda_{\rm PT}/\sigma_{\rm Pt})G_{\rm r}\tanh\left(t_{\rm Pt}/\lambda_{\rm Pt}\right)}\frac{\sigma_{\rm Pt}q_{\rm REE}}{2\sqrt{2}}, \quad (8)$$

where σ_s is the conductivity of the Pt surface. Assuming $\sigma_s = \sigma_{\rm Pt}$, we obtain $q_{\rm REE} = 0.045\ {\rm nm}^{-1}$ for the surface Rashba state of Pt. This value is comparable to $q_{\rm REE}$ for other Rashba systems, such as the interfaces between a nonmagnetic metal and indium tin oxide [41].

Using the obtained parameters, we also calculate the Pt-layer thickness $t_{\rm Pt}$ dependence of $\xi^E_{\rm DL,bulk}$, $\xi^E_{\rm DL,surface}$, and $\beta = \xi^E_{\rm DL,bulk}/(\xi^E_{\rm DL,bulk} + \xi^E_{\rm DL,surface})$ for Pt/Co bilayers, as shown in Figs. 2(g) and 2(h). For the calculation, we take into account the $t_{\rm Pt}$ dependence of the Pt-layer resistivity $\rho_{\rm Pt}$ [see the inset to Fig. 2(h)] [24].

Figures 2(g) and 2(h) demonstrate that the surface contribution is significant only when $t_{\rm Pt} < 3$ nm. In fact, we confirm that $\xi^E_{\rm DL}$ measured for a Pt/Co bilayer with $t_{\rm Pt} = 10$ nm is not affected by the SAM formation. The negligible contribution from $\xi^E_{\rm DL,surface}$ to $\xi^E_{\rm DL}$ when $t_{\rm Pt} > 3$ nm is consistent with previous reports where the surface effect has been neglected.

From the measured values of $\xi^E_{\rm DL}$ shown in Table I, we obtain $\xi^E_{\rm DL,surface} = 1.91 \times 10^4\ \Omega^{-1}{\rm m}^{-1}$ for the PFDT-Pt/Co and $\xi^E_{\rm DL,surface} = 1.00 \times 10^4\ \Omega^{-1}{\rm m}^{-1}$ for the ODT-Pt/Co under the assumption that the $\xi^E_{\rm DL,bulk}$ is unchanged by the molecular self-assembly, which is supported by the negligible change of $\rho_{\rm Pt}$. This result shows that the PFDT formation enhances the surface Rashba-Edelstein SOT efficiency $\xi^E_{\rm DL,surface}$ by 39%, while the ODT formation suppresses $\xi^E_{\rm DL,surface}$ by 27%. The enhanced(suppressed) surface Rashba effect induced by the PFDT(ODT) formation is supported by spin-pumping experiments (see the Supplemental Material [31]).

IV. DENSITY-FUNCTIONAL-THEORY CALCULATIONS

To reveal the mechanism of the molecular tuning of the surface Rashba-Edelstein SOT, we perform plane-wave-based density-functional-theory (DFT)

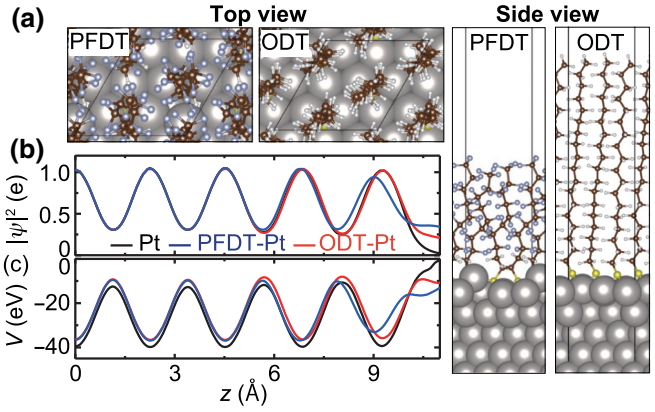

FIG. 3. (a) The top view and side view of the optimized geometries of PFDT- and ODT-adsorbed surfaces. The brown, yellow, blue, white, and gray spheres represent C, S, F, H, and Pt atoms, respectively. The unit cell is shown by the solid line. (b) The planar-averaged charge density $|\psi|^2$ and (c) the electric potential V for Pt (black), PFDT-Pt (blue), and ODT-Pt (red). The coordinate represents the z axis.

calculations using the VASP software package [42]. We assume the ODT- and PFDT-adsorbed surface structure to consist of $(\sqrt{3} \times \sqrt{3})R30^\circ$ unit cells (see Fig. 3 and the Supplemental Material [31]). This surface structure is often found in thiol-adsorbed Pt surfaces [43]. The Bayesian error estimation functional with van der Waals correlation (BEEF-vdW) is used [44] and the plane-wave cutoff is set to 400 and 500 eV for the geometry optimization and electrostatic potential calculations, respectively. We place approximately 15-Å vacuum layers between the surface slabs and a $6 \times 6 \times 1$ k point is used for the reciprocal space integration.

The calculation reveals that the manipulation of the surface Rashba-Edelstein effect is induced by molecular tuning of the wave-function asymmetry and the electrostatic potential near the Pt surface. At metal surfaces, the symmetry-breaking surface potential distorts the atomic orbitals through the admixture with the other orbitals, giving rise to asymmetric wave functions close to the nucleus, where the spin-orbit coupling is strong [45–48]. The wave-function asymmetry plays a key role in the Rashba physics [46]. In fact, tight-binding calculations have shown that the strength of the Rashba spin-orbit coupling is determined by the asymmetry of the surface-state wave function near the position of the nucleus, in combination with the atomic spin-orbit coupling [47]. In Fig. 3(a), we show the optimized geometry of the PFDT- and ODT-adsorbed surfaces. For the optimized structure, we calculate the planar-averaged charge density and the planar-averaged electrostatic potential as shown in Figs. 3(b) and 3(c). This result shows that both the change density and the electrostatic potential close to the Pt surface are modulated by the SAM formation.

In plane-wave-based calculations, the Rashba parameter can be expressed as [49]

$$\alpha_{\mathrm{R}} = \frac{\hbar^2}{4m^2c^2} \int \frac{\partial V}{\partial z} |\psi|^2 \, dz, \tag{9}$$

where c, $\partial V/\partial z$, and $|\psi|^2$ are the speed of light, the potential gradient, and the electron density distribution, respectively. Equation (9) indicates that the asymmetry of the charge-density distribution and the potential gradient gives rise to the Rashba spin-orbit coupling. Using Eq. (9) with the charge-density distribution and electrostatic potential shown in Figs. 3(b) and 3(c), we calculate the Rashba parameter. The calculation shows that the Rashba parameter $\alpha_{\mathrm{R}}^{\mathrm{Pt}}$ of the Pt surface is enhanced by the PFDT formation, while it is decreased by the ODT formation: $\alpha_{\mathrm{R}}^{\mathrm{PFDT\text{-}Pt}}/\alpha_{\mathrm{R}}^{\mathrm{Pt}} = 1.4$ and $\alpha_{\mathrm{R}}^{\mathrm{ODT\text{-}Pt}}/\alpha_{\mathrm{R}}^{\mathrm{Pt}} = 0.94$, where $\alpha_{\mathrm{R}}^{\mathrm{PFDT(ODT)\text{-}Pt}}$ is the Rashba parameter of the PFDT(ODT)-Pt. Although the ODT-induced change of α_{R} in this simple model is smaller than the experimental value, this result is qualitatively consistent with the enhanced(suppressed) surface Rashba-Edelstein SOT induced by the PFDT(ODT) formation.

The calculation shows that both the PFDT and ODT formation on the Pt surface induce the transfer of electrons from the Pt to the molecule; 0.320 electrons per Pt atom are transferred to PFDT and 0.268 electrons per Pt atom are transferred to ODT. This indicates that the electron transfer alone cannot explain the fact that the PFDT formation enhances α_{R}, while the ODT formation suppresses α_{R}. We note that the change of α_{R} due to the PFDT formation is strongly affected by the out-of-plane buckling of Pt atoms; as shown in Fig. 3(a), a Pt atom of the outermost surface adsorbed by PFDT is protruding upward while other atoms are pushed into the bulk. Such surface reconstruction is insignificant in ODT-Pt. This surface reconstruction can be conjectured to optimize the hybridization of the (s, p_z) surface state of PFDT-Pt. The buckling of surface atoms has been shown to play an important role in the realization of strong spin splitting, such as in heavy-metal–Ag(111) and 2D-honeycomb systems [50,51]. Interface phenomena manipulated by molecular layers have been investigated in the field of so-called "spinterface science" [52,53]. The research in this field mainly focuses on manipulation of the magnetic properties of ferromagnetic metals, such as the magnetic anisotropy and the spin polarization. Our result demonstrates that organic molecules also provide a way to control the SOTs in metallic heterostructures, extending the research fields of spinterface science and spin orbitronics.

V. CONCLUSIONS

In summary, we demonstrate that the surface Rashba-Edelstein effect generates a sizable SOT. We note that the

surface Rashba-Edelstein SOT has not been observed even in Pt, the most fundamental and widely used heavy metal in spin orbitronics. We also note that despite the theoretical prediction of a strong Rashba effect [54], the observation of Rashba spin splitting at Pt surfaces using photoelectron spectroscopy is still lacking. Our discovery of the surface Rashba-Edelstein SOT in the prototypical spin-orbitronic system alters the landscape of SOT generation, promising significant advances in the spin-orbit physics of solid-state devices.

ACKNOWLEDGMENTS

This work was supported by the Japan Society for the Promotion of Science (JSPS) Grants-in-Aid for Scientific Research (KAKENHI) under Grants No. 19H00864, No. 26220604, No. 26103004, No. 18J20780, and No. 17H04808 and by the Asahi Glass Foundation, the Kao Foundation for Arts and Sciences, the Canon Foundation, the JGC-S Scholarship Foundation, and the Spintronics Research Network of Japan (Spin-RNJ).

[1] B. Dieny and M. Chshiev, Perpendicular magnetic anisotropy at transition metal/oxide interfaces and applications, Rev. Mod. Phys. **89**, 025008 (2017).

[2] F. Hellman *et al.*, Interface-induced phenomena in magnetism, Rev. Mod. Phys. **89**, 025006 (2017).

[3] J. Sinova, S. O. Valenzuela, J. Wunderlich, C. H. Back, and T. Jungwirth, Spin Hall effects, Rev. Mod. Phys. **87**, 1213 (2015).

[4] Y. Niimi and Y. Otani, Reciprocal spin Hall effects in conductors with strong spin-orbit coupling: A review, Rep. Prog. Phys. **78**, 124501 (2015).

[5] A. Manchon, J. Železný, I. M. Miron, T. Jungwirth, J. Sinova, A. Thiaville, K. Garello, and P. Gambardella, Current-induced spin-orbit torques in ferromagnetic and antiferromagnetic systems, Rev. Mod. Phys. **91**, 035004 (2019).

[6] A. Hoffmann, Spin Hall effects in metals, IEEE Trans. Magn. **49**, 5172 (2013).

[7] A. Manchon, H. C. Koo, J. Nitta, S. M. Frolov, and R. A. Duine, New perspectives for Rashba spin-orbit coupling, Nat. Mater. **14**, 871 (2015).

[8] A. Soumyanarayanan, N. Reyren, A. Fert, and C. Panagopoulos, Emergent phenomena induced by spin-orbit coupling at surfaces and interfaces, Nature **539**, 509 (2016).

[9] E. I. Rashba, Properties of semiconductors with an extremum loop. 1. Cyclotron and combinational resonance in a magnetic field perpendicular to the plane of the loop, Sov. Phys. Solid State **2**, 1109 (1960).

[10] J. Nitta, T. Akazaki, H. Takayanagi, and T. Enoki, Gate Control of Spin-Orbit Interaction in an Inverted $In_{0.53}Ga_0.47As/In_0.52Al_0.48As$ Heterostructure, Phys. Rev. Lett. **78**, 1335 (1997).

[11] C. R. Ast, J. Henk, A. Ernst, L. Moreschini, M. C. Falub, D. Pacilé, P. Bruno, K. Kern, and M. Grioni, Giant Spin Splitting through Surface Alloying, Phys. Rev. Lett. **98**, 186807 (2007).

[12] S. LaShell, B. A. McDougall, and E. Jensen, Spin Splitting of an Au(111) Surface State Band Observed with Angle Resolved Photoelectron Spectroscopy, Phys. Rev. Lett. **77**, 3419 (1996).

[13] A. Varykhalov, D. Marchenko, M. R. Scholz, E. D. L. Rienks, T. K. Kim, G. Bihlmayer, J. Sánchez-Barriga, and O. Rader, Ir(111) Surface State with Giant Rashba Splitting Persists under Graphene in Air, Phys. Rev. Lett. **108**, 066804 (2012).

[14] V. M. Edelstein, Spin polarization of conduction electrons induced by electric current in two-dimensional asymmetric electron systems, Solid State Commun. **73**, 233 (1990).

[15] V. V. Bel'kov and S. D. Ganichev, Magneto-gyrotropic effects in semiconductor quantum wells, Semicond. Sci. Technol. **23**, 114003 (2008).

[16] I. M. Miron, K. Garello, G. Gaudin, P.-J. Zermatten, M. V. Costache, S. Auffret, S. Bandiera, B. Rodmacq, A. Schuhl, and P. Gambardella, Perpendicular switching of a single ferromagnetic layer induced by in-plane current injection, Nature **476**, 189 (2011).

[17] L. Liu, C.-F. Pai, Y. Li, H. W. Tseng, D. C. Ralph, and R. A. Buhrman, Spin-torque switching with the giant spin Hall effect of tantalum, Science **336**, 555 (2012).

[18] G. Yu, P. Upadhyaya, Y. Fan, J. G. Alzate, W. Jiang, K. L. Wong, S. Takei, S. A. Bender, L.-T. Chang, Y. Jiang, M. Lang, J. Tang, Y. Wang, Y. Tserkovnyak, P. K. Amiri, and K. L. Wang, Switching of perpendicular magnetization by spin-orbit torques in the absence of external magnetic fields, Nat. Nanotechnol. **9**, 548 (2014).

[19] H. Kurebayashi, J. Sinova, D. Fang, A. C. Irvine, T. D. Skinner, J. Wunderlich, V. Novák, R. P. Campion, B. L. Gallagher, E. K. Vehstedt, L. P. Zârbo, K. Výborný, A. J. Ferguson, and T. Jungwirth, An antidamping spin-orbit torque originating from the Berry curvature, Nat. Nanotechnol. **9**, 211 (2014).

[20] S. Fukami, C. Zhang, S. DuttaGupta, A. Kurenkov, and H. Ohno, Magnetization switching by spin-orbit torque in an antiferromagnet-ferromagnet bilayer system, Nat. Mater. **15**, 535 (2016).

[21] P. Gambardella and I. M. Miron, Current-induced spin-orbit torques, Phil. Trans. R. Soc. A **369**, 3175 (2011).

[22] R. Ramaswamy, J. M. Lee, K. Cai, H. Yang, and Recent advances in spin-orbit torques, Moving towards device applications, Appl. Phys. Rev. **5**, 031107 (2018).

[23] H. Nakayama, T. Yamamoto, H. An, K. Tsuda, Y. Einaga, and K. Ando, Molecular engineering of Rashba spin-charge converter, Sci. Adv. **4**, eaar3899 (2018).

[24] P. Fan, K. Yi, J.-D. Shao, and Z.-X. Fan, Electrical transport in metallic films, J. Appl. Phys. **95**, 2527 (2004).

[25] S. Onclin, B. J. Ravoo, and D. N. Reinhoudt, Engineering silicon oxide surfaces using self-assembled monolayers, Angew. Chem. Int. Ed. **44**, 6282 (2005).

[26] B. de Boer, A. Hadipour, M. M. Mandoc, T. van Woudenbergh, and P. W. M. Blom, Tuning of metal work functions with self-assembled monolayers, Adv. Mater. **17**, 621 (2005).

[27] J. H. Fendler, Chemical self-assembly for electronic applications, Chem. Mater. **13**, 3196 (2001).

[28] H. Ma, H.-L. Yip, F. Huang, and A. K.-Y. Jen, Interface engineering for organic electronics, Adv. Funct. Mater. **20**, 1371 (2010).
[29] J. C. Love, L. A. Estroff, J. K. Kriebel, R. G. Nuzzo, and G. M. Whitesides, Self-assembled monolayers of thiolates on metals as a form of nanotechnology, Chem. Rev. **105**, 1103 (2005).
[30] A. Ulman, Formation and structure of self-assembled monolayers, Chem. Rev. **96**, 1533 (1996).
[31] See the Supplemental Material for http://link.aps.org/supplemental/10.1103/PhysRevApplied.13.044069 a detailed description of the x-ray photoelectron spectroscopy, the inverse Rashba-Edelstein effect induced by spin pumping, and the density-functional-theory calculations, which includes Refs. [55–59].
[32] C.-F. Pai, Y. Ou, L. H. Vilela-Leão, D. C. Ralph, and R. A. Buhrman, Dependence of the efficiency of spin Hall torque on the transparency of Pt/ferromagnetic layer interfaces, Phys. Rev. B **92**, 064426 (2015).
[33] L. Liu, T. Moriyama, D. C. Ralph, and R. A. Buhrman, Spin-Torque Ferromagnetic Resonance Induced by the Spin Hall Effect, Phys. Rev. Lett. **106**, 036601 (2011).
[34] W. Zhang, W. Han, X. Jiang, S.-H. Yang, and S. S. P. Parkin, Role of transparency of platinum-ferromagnet interfaces in determining the intrinsic magnitude of the spin Hall effect, Nat. Phys. **11**, 496 (2015).
[35] V. Tshitoyan, C. Ciccarelli, A. P. Mihai, M. Ali, A. C. Irvine, T. A. Moore, T. Jungwirth, and A. J. Ferguson, Electrical manipulation of ferromagnetic NiFe by antiferromagnetic IrMn, Phys. Rev. B **92**, 214406 (2015).
[36] M.-H. Nguyen, D. C. Ralph, and R. A. Buhrman, Spin Torque Study of the Spin Hall Conductivity and Spin Diffusion Length in Platinum Thin Films with Varying Resistivity, Phys. Rev. Lett. **116**, 126601 (2016).
[37] V. P. Amin and M. D. Stiles, Spin transport at interfaces with spin-orbit coupling: Phenomenology, Phys. Rev. B **94**, 104420 (2016).
[38] A. Kalitsov, S. A. Nikolaev, J. Velev, M. Chshiev, and O. Mryasov, Intrinsic spin-orbit torque in a single-domain nanomagnet, Phys. Rev. B **96**, 214430 (2017).
[39] S. Dushenko, M. Hokazono, K. Nakamura, Y. Ando, T. Shinjo, and M. Shiraishi, Tunable inverse spin Hall effect in nanometer-thick platinum films by ionic gating, Nat. Commun. **9**, 3118 (2018).
[40] E. Sagasta, Y. Omori, M. Isasa, M. Gradhand, L. E. Hueso, Y. Niimi, Y. Otani, and F. Casanova, Tuning the spin Hall effect of Pt from the moderately dirty to the superclean regime, Phys. Rev. B **94**, 060412(R) (2016).
[41] K. Kondou, H. Tsai, H. Isshiki, and Y. Otani, Efficient spin current generation and suppression of magnetic damping due to fast spin ejection from nonmagnetic metal/indium-tin-oxide interfaces, APL Mater. **6**, 101105 (2018).
[42] G. Kresse and J. Furthmüller, Efficient iterative schemes for *ab initio* total-energy calculations using a plane-wave basis set, Phys. Rev. B **54**, 11169 (1996).
[43] C. Vericat, M. E. Vela, G. Corthey, E. Pensa, E. Cortés, M. H. Fonticelli, F. Ibañez, G. E. Benitez, P. Carro, and R. C. Salvarezza, Self-assembled monolayers of thiolates on metals: A review article on sulfur-metal chemistry and surface structures, RSC Adv. **4**, 27730 (2014).
[44] J. Wellendorff, K. T. Lundgaard, A. Møgelhøj, V. Petzold, D. D. Landis, J. K. Nørskov, T. Bligaard, and K. W. Jacobsen, Density functionals for surface science: Exchange-correlation model development with Bayesian error estimation, Phys. Rev. B **85**, 235149 (2012).
[45] K. V. Shanavas, Z. S. Popović, and S. Satpathy, Theoretical model for Rashba spin-orbit interaction in *d* electrons, Phys. Rev. B **90**, 165108 (2014).
[46] L. Petersen and P. Hedegård, A simple tight-binding model of spin-orbit splitting of *sp*-derived surface states, Surf. Sci. **459**, 49 (2000).
[47] G. Bihlmayer, Y. M. Koroteev, P. M. Echenique, E. V. Chulkov, and S. Blügel, The Rashba-effect at metallic surfaces, Surf. Sci. **600**, 3888 (2006).
[48] O. Krupin, G. Bihlmayer, K. Starke, S. Gorovikov, J. E. Prieto, K. Döbrich, S. Blügel, and G. Kaindl, Rashba effect at magnetic metal surfaces, Phys. Rev. B **71**, 201403(R) (2005).
[49] M. Nagano, A. Kodama, T. Shishidou, and T. Oguchi, A first-principles study on the Rashba effect in surface systems, J. Phys. Condens. Matter **21**, 064239 (2009).
[50] G. Bihlmayer, S. Blügel, and E. V. Chulkov, Enhanced Rashba spin-orbit splitting in BiAg(111) and PbAg(111) surface alloys from first principles, Phys. Rev. B **75**, 195414 (2007).
[51] P. Z. Hanakata, A. S. Rodin, A. Carvalho, H. S. Park, D. K. Campbell, and A. H. Castro Neto, Two-dimensional square buckled Rashba lead chalcogenides, Phys. Rev. B **96**, 161401(R) (2017).
[52] S. Sanvito, Molecular spintronics: The rise of spinterface science, Nat. Phys. **6**, 562 (2010).
[53] M. Cinchetti, V. A. Dediu, and L. E. Hueso, Activating the molecular spinterface, Nat. Mater. **16**, 507 (2017).
[54] A. Bendounan, K. Aït-Mansour, J. Braun, J. Minár, S. Bornemann, R. Fasel, O. Gröning, F. Sirotti, and H. Ebert, Evolution of the Rashba spin-orbit-split Shockley state on Ag/Pt(111), Phys. Rev. B **83**, 195427 (2011).